Check for updates

Batteries & Supercaps

Research Article
doi.org/10.1002/batt.202300301

Chemistry Europe
European Chemical Societies Publishing

www.batteries-supercaps.org

Evaluation of Asymmetric Flow Rates for Better Performance Vanadium Redox Flow Battery

Abdulmonem Fetyan,*[a] Musbaudeen O. Bamgbopa,[a] Anugrah Andisetiawan,[a] Ayoob Alhammadi,[a] and Rahmat A. Susantyoko[a]

Electrolyte imbalance caused by water and ion crossover is one of the main factors affecting the capacity of vanadium redox flow battery system over cycling. Ion crossover and the associated water transfer towards the positive half-cell is mainly caused by the transfer of the vanadium ions, its bounded water and the water driven by osmosis. The different viscosity of the vanadium (III) ions in the negative half-cell builds inconsistent pressure profiles at both half-cells during charge-discharge cycling and therefore magnifies ions and water transfer tendency. To mitigate the effect of electrolyte imbalance, herein we report an experimental study on the effect of using asymmetric flow rates in the negative and positive half-cells. Over different current densities of 50, 100, and 150 mA cm^{-2}, the use of one magnitude flow factor lower in the negative half-cell and one magnitude flow factor higher in the positive half-cell is superior to the symmetric flow rates on reducing electrolyte imbalance and subsequently, improving the capacity retention. At 100 mA cm^{-2}, a gain of 5% in discharge capacity coupled with energy efficiency improvement of around 3% is achieved using a cell with asymmetric flow rates compared to a cell with the symmetric flow rates after 50 cycles. Low magnitude of flow rate asymmetry can sufficiently compensate for the half-cells pressures imbalance, higher increment in flow rate asymmetry showed that positive-to-negative crossover become more favourable.

Introduction

Redox flow batteries (RFBs) have attracted high attention in large scale energy storage due to their decoupled power and energy capacity.[1,2] Even though there exist utility-scale installations worldwide, the technology's market share is limited due to low energy density and system efficiency compared to other energy systems.[3] The use of circulating pumps in vanadium redox flow battery (VRFB) system to circulate the electrolytes between storage tanks and reaction cells incurs pumping power losses.[4] High constant flow rates are generally reported in vanadium redox flow batteries to achieve high stack energy efficiency. However, this lowers the overall system efficiency as the associated pumping power is increased.[5] Various approaches to optimize the flow rates are reported in the literature. Ma et al.[6] described a pre-defined constant flow rate based on the voltage level of kilo-watt system to optimize the system efficiency and achieve high capacity by having low flow rate followed by higher flow rate to reduce concentration polarization at the end of charge and discharge cycles. Ling et al.[7] proposed a pulsating electrolyte flow strategy to decrease the pump energy consumption. Other research groups demonstrated numerous studies on developing simulation models for better flow rate optimization mainly based on dynamic flow rate which is based on the stoichiometry of the electrolytes.[8–12] Tang et al. proposed an optimal flow rate strategy by defining a constant flow factor as a function of the state of charge (SOC) and applied current.[5] Other research groups developed multi-physics battery models utilizing dynamic flow factor contingent on SOC and power.[13,14]

Preferential water transfer is a common undesirable phenomenon associated with ion exchange membranes in VRFBs, together with vanadium ion crossover and gassing parasitic reactions it will lead to imbalance of the electrolyte and SOC between the two half-cells and eventually capacity fade over cycling.[15] In addition to that, the different viscosity of the vanadium (III) ions in the negative half-cell builds inconsistent pressure profiles at both half-cells and therefore magnifies ions and water transfer tendency. The most common approach to minimize the resulting capacity fade is by improving the ion selectivity of such membranes.[16] However, Li and co-workers[17] reported online monitoring of the SOC in VRFB which can be used to assist in the management of capacity restoration. Song et al.[18,19] reported the impact of viscosity on the electrolyte volumetric transfer in redox flow batteries and suggested a flow rate optimization strategy for both half-cells based on the measurements of electrolyte viscosities. Recent works have addressed the problem differently by using differential initial anolyte/catholyte vanadium concentrations[20] or supporting electrolyte concentrations.[21] Nevertheless, the effect of crossover after long cycling operation persists. Other volume and SOC imbalance remediation methods during cycling like applying reflow[22] or hydraulic shunt[23] often discard the momentarily charge loss at the reflow/rebalance cycle in the grander performance comparison improvement calculations. The approach proposed herein can be used to further improve

[a] Dr. A. Fetyan, Dr. M. O. Bamgbopa, A. Andisetiawan, A. Alhammadi, Dr. R. A. Susantyoko
Research & Development Centre
Dubai Electricity and Water Authority (DEWA)
P.O. Box 564, Dubai (United Arab Emirates)
E-mail: abdulmonem.fetyan@dewa.gov.ae

Supporting information for this article is available on the WWW under https://doi.org/10.1002/batt.202300301

© 2023 Wiley-VCH GmbH

Research Article
doi.org/10.1002/batt.202300301
Chemistry Europe
European Chemical Societies Publishing

their potency. The use of inhomogeneous or asymmetric cell/electrode compression studies also targets similar performance improvement results by affecting crossover, among other factors. Yue Lu et al.[24] through modelling were able to find a mismatched electrode compression ratio and flow field design performance which improved net discharge power between 3.3% to 5.4%. This was mostly due to gains in reaction enhancement (housing the effect of crossover). Lesser gains were reported in pumping power, while ohmic drop was largely unaffected. These performance improvements are also argued to be primarily due to crossover reduction in other studies who also applied asymmetric electrode compression and variable electrode porosity for both sides of VRFBs.[25,26] Our proposed approach here is more simplistic and less costly – as it doesn't require cell architecture modification.

In this paper, we report two approaches to minimize the electrolyte imbalance, a thorough evaluation of the influence of using asymmetric temperature at 100 mA cm^{-2} as well as asymmetric flow rates in the negative and positive half-cells at different current densities and its long-term effect on the VRFB capacity and efficiency. The work provides a good understanding of the limitation of using asymmetric flow rates by analysing the performance of VRFB system and its dependence on crossover and pressure drop and therefore an easy and straightforward pathway to mitigate the effect of electrolyte imbalance caused by the electrolyte's different physical properties.

Results and Discussion

Determination of optimum electrolyte flow rate

Electrolyte circulation flow rate is a key factor for determining the battery's achievable capacity. Recent studies demonstrated an increased capacity by increasing electrolyte flow rate.[5,27–30] However, a higher flow rate requires an increased pumping power which necessitates a decrease in system efficiency. The theoretical flow rate is usually calculated using Equation (1).

$$Q = \lambda \frac{I}{n \cdot F \cdot C \cdot \mathrm{SOC}} \quad (1),$$

where Q is the flow rate (L cm^{-2} h^{-1}), λ is the flow factor (considered 1 for theoretical flow rate), I is the applied current density (A cm^{-2}), n is the electrons involved in the redox reaction, F is Faraday constant (A h mol^{-1}), C is reactant concentration (mol L^{-1}), and SOC is the state of charge.

In order to determine the required flow factor of the system, we tested the cell at three different current densities (50, 100, and 150 mA cm^{-2}) with different flow rates (calculated at 90% SOC using a flow factor of 2, 4, 8, 12, 16, 20 and 24 at each current density). Figure 1 presents the coulombic efficiency, energy efficiency, and achievable discharge capacity for the three current densities at different flow rates. As shown in Figure 1(a), the use of a low flow rate of 2 mL min^{-1} for the cell tested at a current density of a 50 mA cm^{-2} showed poor performance in terms of efficiencies and discharge capacity, increasing the flow rate to 4 mL min^{-1} by applying the flow rate factor of 2 revealed significant improvement in coulombic efficiency (CE) and energy efficiency (EE) and discharge capacity (detailed data are shown in Table S1). While the CE and EE showed similar values when increasing the flow rate to 16 mL min^{-1}, the achievable capacity demonstrated a noticeable increase of around 11%. Further increment of the flow rate factor demonstrated steady values of both CE and EE while the achievable capacity only showed slight improvement. Figure 1(b and c) shows poor CE, EE, and achievable capacity at the low flow rate of 4 mL min^{-1} and 6 mL min^{-1} for both current densities of 100 and 150 mA cm^{-2}, respectively. The first increment in the flow factor exhibited improvement in all values, where the CE reached 96% and 94%, the EE exhibited 68% and 56%, and the achievable discharge capacity showed 65% and 41% for 100 and 150 mA cm^{-2}, respectively. Further increase in the flow factor for both 100 mA cm^{-2} and 150 mA cm^{-2} showed the same trend observed for the low current density of 50 mA cm^{-2} where both CE and EE presented constant values, and the capacity achieved higher percentages. From these observations, a general conclusion can be given that, higher flow rates are preferred to overcome the mass transport limitation). However, for all current densities, the major increase in capacity occurs when flow factor of up to 8 is used (see Figure 1 and Table S1). Higher flow factors exhibit minor increment in capacity (less than 3% per each increase of the flow factor), indicating that a flow factor between 4 and 8

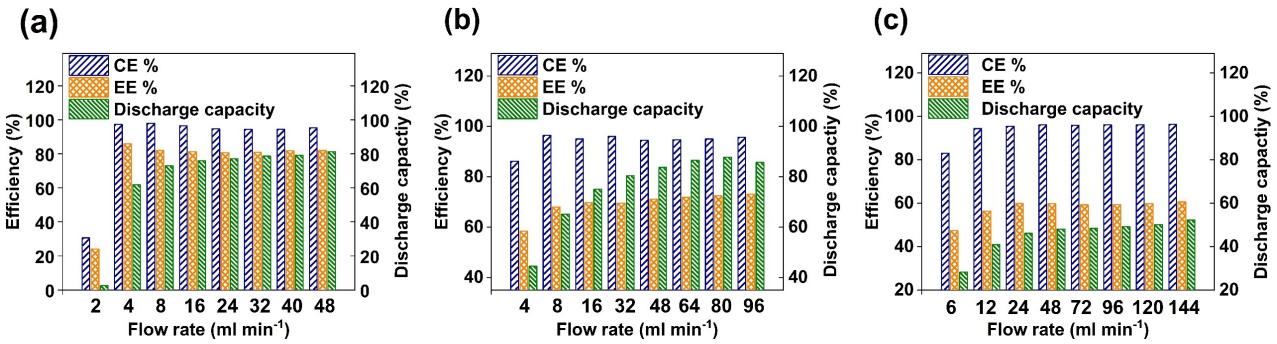

Figure 1. Average coulombic efficiency, energy efficiency, and discharge capacity (calculated as the percentage of the theoretical capacity) recorded for two galvanostatic charge-discharge cycles tested at a) 50 mA cm^{-2}, b) 100 mA cm^{-2}, and c) 150 mA cm^{-2}.

© 2023 Wiley-VCH GmbH

25666223, 2023, 11, Downloaded from https://chemistry-europe.onlinelibrary.wiley.com/doi/10.1002/batt.202300301 by University of Ulsan, Wiley Online Library on [11/11/2025]. See the Terms and Conditions (https://onlinelibrary.wiley.com/terms-and-conditions) on Wiley Online Library for rules of use; OA articles are governed by the applicable Creative Commons License

Research Article
doi.org/10.1002/batt.202300301
Chemistry Europe
European Chemical Societies Publishing

seems to be an optimum value which is in line with previously reported studies.[5,32] To study the effect of asymmetric flow rates between the negative and positive half-cells of the battery, a flow factor of 8 is used to ensure reliable performance at all current densities.

Effect of asymmetric flow rate on capacity and efficiencies

Previous studies reported that the two main reasons for water transfer towards the positive side are the transfer of water driven by osmosis and bound water of vanadium ions.[15,33,34] Using a lower flow rate on the negative side should reduce the elevated pressure induced by the higher viscosity of V(III) compared to V(II), V(IV), and V(V) and therefore is expected to compensate for the water transfer towards the positive side driven by osmosis. In this study, a flow factor of 8 is used for all three current densities in the reference cell for both half-cells. While for the cell with asymmetric flow rates, a theoretical value of flow rate is added to the positive half-cell flow rate and subtracted from the negative half-cell for each current density to introduce higher pressure on the positive side with respect to the negative side.

Figure 2 presents the coulombic efficiency and energy efficiency at different current densities for a reference cell using symmetric flow rates at both half-cells and a cell tested with asymmetric flow rates at positive and negative half-cells. For all current densities, both cells demonstrated similar and stable CE values over cycling with around 96%, for both 50 mA cm^{-2} and 100 mA cm^{-2} and 97% for 150 mA cm^{-2}. Unlike the CE, the EE profiles at all current densities showed the same trend of a slight decrease of efficiency over cycling. At 50 mA cm^{-2} both cells exhibit 82% EE in the first few cycles, a minor decrease is noticed after 25 cycles where it reached 79% and 81% for the cell with the symmetric flow rates and asymmetric flow rates, respectively (see Figure 2a). At current densities of 100 mA cm^{-2} and 150 mA cm^{-2} the cell with symmetric flow rates similarly showed higher regression in EE of around 3%–4% over cycling compared to the cell with asymmetric flow rates (2%).

Figure 3 shows the discharge capacity of the same cells tested at three different current densities shown in Figure 2. As seen in Figure 3, similar behaviour is observed for the cell with asymmetric flow rates at all current densities. The cells with symmetric flow rates exhibit almost the same capacity compared to the cells with asymmetric flow rates for the first 7 cycles at 50 mA cm^{-2} and 16 cycles at 100 mA cm^{-2}. After that

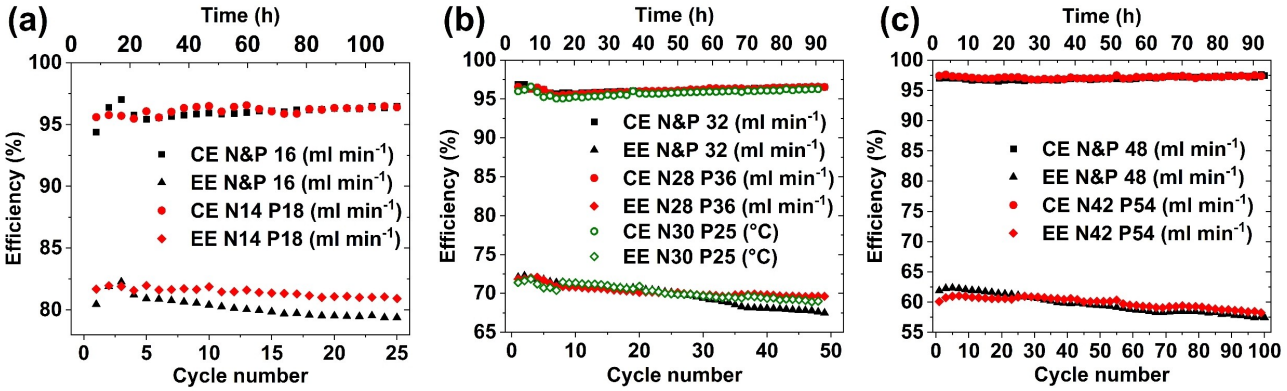

Figure 2. Coulombic efficiency and energy efficiency recorded for galvanostatic charge-discharge cycles for a reference cell using symmetric flow rates and a cell with asymmetric flow rates at positive and negative half-cells tested at three different current densities of a) 50 mA cm^{-2} b) 100 mA cm^{-2} and c) 150 mA cm^{-2}. For b) the third cell is tested with different temperatures at the same flow rate of 32 mL min^{-1} for both half-cells.

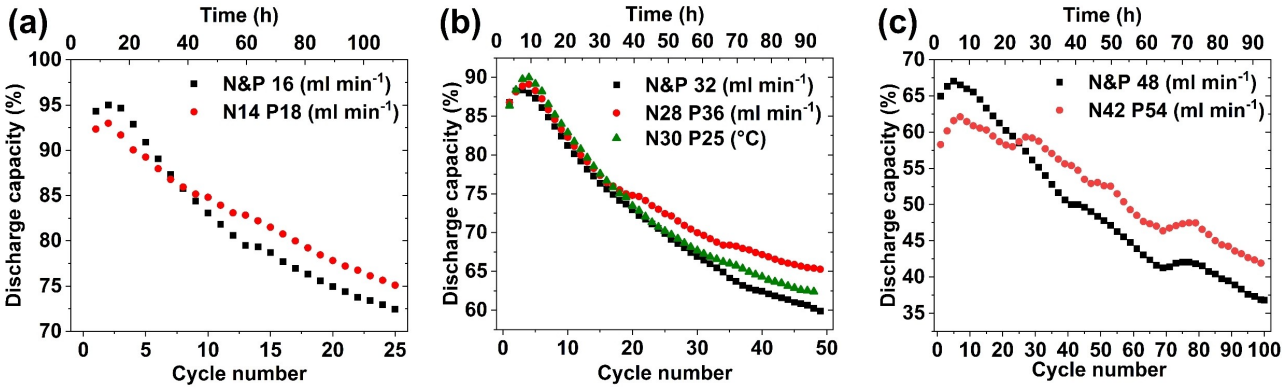

Figure 3. Discharge capacity (calculated as a percentage of the theoretical capacity) for galvanostatic charge-discharge cycles for a reference cell using symmetric flow rates and a cell with asymmetric flow rates at positive and negative half-cells tested at three different current densities of a) 50 mA cm^{-2}, b) 100 mA cm^{-2}, and c) 150 mA cm^{-2}. For b) the third cell is tested with different temperatures at the same flow rate of 32 mL min^{-1} for both half-cells.

© 2023 Wiley-VCH GmbH

25666223, 2023, 11, Downloaded from https://chemistry-europe.onlinelibrary.wiley.com/doi/10.1002/batt.202300301 by University of Ulsan, Wiley Online Library on [11/11/2025]. See the Terms and Conditions (https://onlinelibrary.wiley.com/terms-and-conditions) on Wiley Online Library for rules of use; OA articles are governed by the applicable Creative Commons License

a prominent decrease in the capacity is noticed for the cells with symmetric flow rates over cycling ending with a lower capacity of around 3% for the former current density and 5% for the latter compared to the cells with asymmetric flow rates. At a higher current density of 150 mA cm^{-2}, the cell with symmetric flow rates showed around 5% higher discharge capacity in the first cycle (this difference could be explained by the internal resistance associated with the assembly of different cells), higher capacity fade is also spotted for the cell with symmetric flow rates at this current density during cycling, the discharge capacity of the cell with asymmetric flow rates reached higher values after 30 cycles and showed around 42% discharge capacity with 5% higher capacity retention after 100 cycles compared to the cell with symmetric flow rates which exhibited only 37%.

As seen in Figures 2 and 3, the performance improvement associated with the use of asymmetric flow rates is time-dependent (as cycling proceeds). Therefore, the performance gain is observed after different cycles depending on the duration of the charge-discharge cycle. As expected, the use of a higher flow rate on the positive side leads to a reverse osmosis effect, which results in a reduced rate of ions and water transfer to the positive side. The electrolyte volume in each half-cell is measured after cycling for all cells at all current densities. A similar pattern of lower electrolyte transfer can be seen for the cells with asymmetric flow rates compared to the cells with symmetric flow rates. Table 1. Summarize the electrolyte volume ratio of negative to positive half-cells after cycling for all cells tested at three current densities.

Effect of asymmetric temperature

Another approach to mitigate the difference of electrolyte viscosity is by using different temperatures. Reynard et al. reported the application of a thermally regenerative electrochemical cycle on the VRFB system and concluded enhanced efficiency and energy density over cycling.[35] However, the study employed the same temperature on both half-cells. The use of higher temperature in the negative electrolyte will lower the electrolyte viscosity and therefore decrease the associated pressure during cycling. Figure 2(b) presents the recorded CE and EE data of 50 charge-discharge cycles of a cell with different temperature profiles (30 °C in the negative half-cell and 25 °C in the positive half-cell) using symmetric flow rates at both half-cells. Despite the slight increase in EE observed for the cell with different temperature profiles after around 28 cycles compared to the cell with the same temperatures, the CE showed around 0.5% lower values over the 50 cycles. This decreased CE can be elucidated by the increased rate of the parasitic side reaction of hydrogen evolution described in our previous publication.[36] In contrast to the CE, the cell exhibited around 2% lower capacity decay after 50 cycles in comparison to the cell with the same temperature (see Figure 3b). However, the improvement observed using elevated temperature in the negative half-cell is limited due to the electrolyte degradation caused by the hydrogen evolution at a higher temperature which can also be noted by the negative to positive electrolyte volume ratio reported in Table 1.

Table 1. Summary of electrolyte volume ratio of negative to positive half-cells after cycling for the cells with symmetric flow rates and asymmetric flow rates.

Current density [mA cm^{-2}]	Flow rate [mL min^{-1}]		Half-cell temperature [°C]	Negative to positive electrolyte volume ratio [%]
50	Negative	14	–	87
	Positive	18	–	
	Negative	16	–	83
	Positive	16	–	
100	Negative	28	–	85
	Positive	36	–	
	Negative	32	–	83
	Positive	32	–	
	Negative	32	30	81
	Positive	32	25	
	Negative	32	25	83
	Positive	32	25	
150	Negative	42	–	86
	Positive	54	–	
	Negative	48	–	83
	Positive	48	–	

© 2023 Wiley-VCH GmbH

25666223, 2023, 11, Downloaded from https://chemistry-europe.onlinelibrary.wiley.com/doi/10.1002/batt.202300301 by University of Ulsan, Wiley Online Library on [11/11/2025]. See the Terms and Conditions (https://onlinelibrary.wiley.com/terms-and-conditions) on Wiley Online Library for rules of use; OA articles are governed by the applicable Creative Commons License

Research Article
doi.org/10.1002/batt.202300301
Chemistry Europe
European Chemical Societies Publishing

25666223, 2023, 11, Downloaded from https://chemistry-europe.onlinelibrary.wiley.com/doi/10.1002/batt.202300301 by University of Ulsan, Wiley Online Library on [11/11/2025]. See the Terms and Conditions (https://onlinelibrary.wiley.com/terms-and-conditions) on Wiley Online Library for rules of use; OA articles are governed by the applicable Creative Commons License

Pressure losses

Averaged pressure drop profiles for the tested cells with symmetric flow rates and asymmetric flow rates are presented in Figure 4. At 50 mA cm^{-2} (see Figure 4a), a stable pressure drop is observed in the negative side over the 25 cycles for both cells of asymmetric flow rates and symmetric flow rates of around 2 kPa for the former and 7 kPa for the latter. In contrast to the negative half-cell, the positive half-cell pressure drop showed increased values over cycling. While the cell with asymmetric flow rates recorded an increase of approximately 2 kPa, the cell with symmetric flow rates exhibited roughly 3.5 kPa at the end of the 25th cycle. Similar scenarios are evident for the other two current densities of 100 mA cm^{-2} (Figure 4b) and 150 mA cm^{-2} (Figure 4c). At 100 mA cm^{-2} the pressure drop rose by 5.5 kPa and 6.5 kPa for the cell with asymmetric flow rates and the cell with symmetric flow rates, respectively. Similarly, the cell with symmetric flow rates demonstrated about 1 kPa higher increment in pressure drop than the cell with asymmetric flow rates at 150 mA cm^{-2} in the positive half-cell. The higher increment in pressure drop observed for the cell with symmetric flow rates in the positive half-cell can be associated with the increased ion and water transfer from the negative half-cell toward the positive half-cell. This elevated pressure drop will necessitate higher pumping power during cycling. Therefore, applying asymmetric flow rates should not only benefit in reducing the electrolyte transfer but also improve the system's overall efficiency by reducing the required pumping power during the charge-discharge process.

Improvements in both energy efficiency and discharge capacity with the asymmetric flow rate scenarios compared to using symmetric flow rates are strongly determined by cross-over as initially proposed and discussed so far. A model for the osmotic water (or bulk electrolyte) crossover rate, Q_{cross} across the membrane can by set-up with a Darcy's law type relationship – neglecting other effects seen in Equation (2).

$$\frac{Q_{cross}}{A} = -\frac{\Delta P}{\mu\, t_{memb}} \tag{2}$$

$$\Delta P = \left(P_{drop,\,neg} - P_{drop,\,pos}\right) \tag{3}$$

where, ΔP is an effective pressure differential for crossover between both sides of the battery defined by inlet-to-outlet pressure drop (P_{drop}) difference, assuming negative to positive [Equation (3)]. μ is an average electrolyte viscosity across the membrane. A and t_{memb} are the cell cross-sectional area and membrane thickness, respectively. $\bar{\kappa}$ - which is an effective

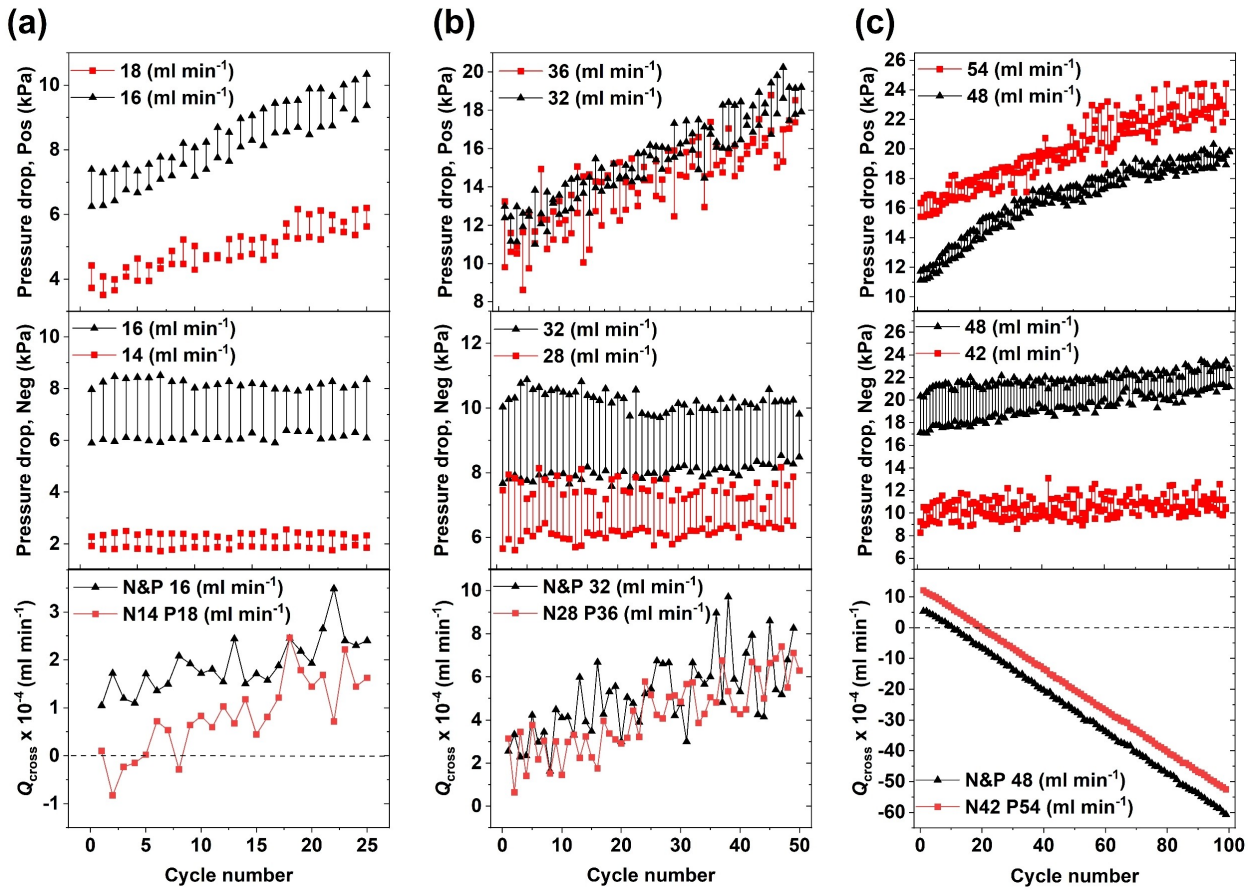

Figure 4. Measured pressure drop profiles recorded (at the beginning and ending of each charge cycle) and estimated crossover rates. a) Symmetric with 16 mL min^{-1} inflow on both sides, or asymmetric with 14 mL min^{-1} inflow on negative & 18 mL min^{-1} inflow on positive at 50 mA cm^{-2}, b) symmetric with 32 ml min^{-1} inflow on both sides, or asymmetric with 28 mL min^{-1} inflow on negative & 36 mL min^{-1} inflow on positive at 100 mA cm^{-2}, and c) symmetric with 48 mL min^{-1} inflow on both sides, or asymmetric with 42 mL min^{-1} inflow on negative & 54 mL min^{-1} inflow on positive at 150 mA cm^{-2}.

© 2023 Wiley-VCH GmbH

hydraulic permeability for crossover was estimated herein as 0.73×10^{-18} m^2 using fluid-flow simulation from our full Multi-physics model presented in earlier work[37] under different flow scenarios (see more details in Supporting Information). The sign convention in Equations (2) and (3) shows that $\Delta P > 0$ gives $Q_{cross} < 0$, indicating a crossover from negative to positive side of the battery. $\Delta P < 0$ gives $Q_{cross} > 0$, indicating the direction of crossover is reversed.

The estimated κ value now helps present the relative crossover rates using the experimentally measured pressure drop profiles for the tested three symmetric/asymmetric flow rates scenarios. Q_{cross} can now be put into perspective in terms of both magnitude and suggested crossover direction. The pressure drops profiles on both sides ($P_{drop,\,neg}$ and $P_{drop,\,pos}$) shown in Figure 4 were measured at the end of charging and discharging at every cycle. Therefore, double values are seen in Figure 4 for each cycle number due to the known variation of VRFB electrolyte hydraulic properties like density and viscosity with SOC.[19] However, we do not unnecessarily complicate our estimation of Q_{cross} by accounting for SOC variation of the fluid properties – given the discrete pressure drop recording at each cycle. The results from Q_{cross} estimation in the three test cases shown in Figure 4(a–c), respectively leads to the following conclusions:

- As expected, the pressure drop on a particular side is generally higher with increasing flow rate. The relationship is more magnified on the negative side due to the higher viscosity of the negative electrolyte – at least in the first few cycles.
- The initially higher viscosity of the negative electrolyte may lead one to erroneously conclude that crossover is always from negative-to-positive side when the inflow rates are symmetric (since negative viscosity is higher). However, the change in electrolyte composition as cycling proceeds (increasing total crossover volume) shows a variation in crossover rate and direction as seen in Figure 4.
- Although the variation of viscosity and density with SOC on both sides is not considered herein, studies which measure these variations[19,38] usually measure the properties with pure electrolytes or generating different SOC electrolytes at theoretical SOCs with electrolytic cells. Notably here that property variation during real (dis)charging cycling better accounts for operando electrolyte composition, is more descriptive of crossover, and would increase the accuracy of state of charge estimation efforts using electrolyte viscosity,[17] or density[39] measurements.

Low magnitude of flow rate asymmetry can sufficiently compensate for the half-cells pressures imbalance and stabilize or reverse the crossover direction at low timeframes, as seen for the first 5 cycles in Figure 4(a). With further increment in the magnitude of flow rate asymmetry (Figure 4b and c), the positive side pressure drop is higher and leads the initial crossover to be positive-to-negative.

Given the above conclusions, the discharge capacity performance improvement with proposed inflow asymmetry (See Figure 3) in this study is explained by the prevalent positive-to-negative crossover direction being more favourable (than negative-to-positive crossover direction) during discharge – given the ensuing desired charge transfer reactions and undesired side reactions due to crossover[33] in Equations (4) to (9).

Conclusions

In this work, various flow factors are evaluated at different current densities. A flow factor between four and eight is an optimum value for achieving the highest capacity and efficiency while keeping the pumping losses minimal. Additionally, two approaches to mitigate the electrolyte imbalance are implemented. Long-term multiple charge-discharge cycles for a cell with asymmetric flow rates at negative and positive half-cells compared to a cell with symmetric flow rates are tested at three different current densities. Applying a lower flow factor in the negative half-cell compared to the positive half-cell reduced the electrolyte migration towards the positive half-cell and therefore decrease capacity fade over cycling. The enhanced performance is time-dependent and can be observed after a different number of cycles depending on the duration of the charge-discharge cycle. For instance, at a current density of 50 mA cm^{-2} the capacity improved after eight cycles, whereas at 150 mA cm^{-2} the improvement was observed after twenty-five cycles. Crossover rate calculation across the membrane demonstrated that low magnitude of flow rate asymmetry can sufficiently compensate for the half-cells pressures imbalance and stabilize or reverse the crossover direction, further increment in the magnitude of flow rate asymmetry showed that positive side pressure drop becomes higher and leads the initial crossover to be positive-to-negative. In the second approach, a higher temperature is employed in the negative half-cell with respect to the positive half-cell. The capacity and energy efficiency enhancement were limited and explained by the increased rate of the parasitic reaction of hydrogen evolution in the negative half-cell at elevated temperature. Pressure drop profiles demonstrated lower pressure drop over cycling in the positive half-cell using asymmetric flow rates compared to the cell with symmetric flow rates, which can be beneficial for lowering the required pumping power. The use of asymmetric flow rates to mitigate electrolyte imbalance can also be applied on other redox flow systems/chemistry. However, the optimum flow factor for each half-cell is highly depending on the electrolyte's physical properties and applied conditions during charging-discharging which requires a detailed investigation and further analysis for each system/chemistry.

Experimental Section

The measurements were conducted using an integrated redox flow cell test system (Test bench 857, Scribner Associates). Single-cell flow-through geometry cell (Micro Flow Cell, Electro Cell Denmark) with 117 Nafion proton-exchange membrane (Ion Power, Inc.), graphite plates current collectors, and heat-treated carbon felts at 400 °C for 10 hours with a nominal thickness of 6 mm and active area of 10 cm^2 (3.3×3 mm size) GFA6 (SGL carbon, Germany) were

© 2023 Wiley-VCH GmbH

25666223, 2023, 11, Downloaded from https://chemistry-europe.onlinelibrary.wiley.com/doi/10.1002/batt.202300301 by University of Ulsan, Wiley Online Library on [11/11/2025]. See the Terms and Conditions (https://onlinelibrary.wiley.com/terms-and-conditions) on Wiley Online Library for rules of use; OA articles are governed by the applicable Creative Commons License

used. A compression rate of 25% of the cell was applied. Vanadium electrolyte (1.6 mol L^{-1} (mixture of V^{3+} and V^{4+}) in 2 mol L^{-1} H_2SO_4 and 0.05 mol L^{-1} H_3PO_4, GFE chemicals) of 30 mL was used as starting electrolyte for both negative and positive tanks. Nitrogen flow of 60 mL min^{-1} was applied in the negative tank to prevent electrolyte oxidation. The used cut-off voltage is 1.7 V for charging and 0.8 V for discharging. Temperature sensors Type T were used for temperature sensing. Pressure transmitters (Sensys PCAH0300RBSA, Rep. of Korea) with 0–300 kPa range and 0.05% full-scale accuracy were utilized at the inlet and outlet of each half-cell to record the pressure before and after the cell, the collected data were then averaged at the beginning and the end of each cycle to normalize the noises from analogue signal conversion and wavery pressure data due to peristaltic pump. Charge-discharge experiments are repeated at least twice to assure the repeatability of data.

CRediT authorship contribution statement

Abdulmonem Fetyan: Conceptualization, Methodology, Investigation, Writing – original draft, Writing – review & editing, Validation, Formal analysis, Visualization. Musbaudeen O. Bamgbopa: Writing – original draft, Writing – review & editing, Formal analysis, Visualization. Anugrah Andisetiawan: Formal analysis. Ayoob Alhammadi: Investigation, Writing - Original Draft. Rahmat A. Susantyoko: Writing - Original Draft, Project administration, Funding acquisition.

Supporting Information

Additional references cited within the Supporting Information.[40]

Conflict of Interests

The authors declare no conflict of interest.

Data Availability Statement

The data that support the findings of this study are available from the corresponding author upon reasonable request.

Keywords: asymmetric flow rates · pumping losses · pressure drop · electrolyte viscosity · vanadium redox flow batteries

[1] R. K. Sankaralingam, S. Seshadri, J. Sunarso, A. I. Bhatt, A. Kapoor, *J. Energy Storage* **2021**, *41*, 102857.
[2] A. Fetyan, I. Derr, M. K. Kayarkatte, J. Langner, D. Bernsmeier, R. Kraehnert, C. Roth, *ChemElectroChem* **2015**, *2*, 2055–2060.
[3] A. Fetyan, J. Schneider, M. Schnucklake, G. A. El-Nagar, R. Banerjee, N. Bevilacqua, R. Zeis, C. Roth, *ChemElectroChem* **2019**, *6*, 130–135.
[4] Q. Ye, J. Hu, P. Cheng, Z. Ma, *J. Power Sources* **2015**, *296*, 352–364.
[5] A. Tang, J. Bao, M. Skyllas-Kazacos, *J. Power Sources* **2014**, *248*, 154–162.
[6] X. Ma, H. Zhang, C. Sun, Y. Zou, T. Zhang, *J. Power Sources* **2012**, *203*, 153–158.
[7] C. Y. Ling, H. Cao, M. L. Chng, M. Han, E. Birgersson, *J. Power Sources* **2015**, *294*, 305–311.
[8] H.-F. Shen, X.-J. Zhu, M. Shao, H. Cao, *J. Appl. Math.* **2013**, *2013*, 538237.
[9] S. König, M. R. Suriyah, T. Leibfried, *The Sixth International Renewable Energy Congress* **2015**, pp. 1–6.
[10] X. Binyu, Z. Jiyun, L. Jinbin, *IEEE Power & Energy Society General Meeting* **2013**, pp. 1–5.
[11] W. Xiao, L. Tan, *Renewable Energy* **2019**, *133*, 1445–1454.
[12] T. Jirabovornwisut, S. Kheawhom, Y.-S. Chen, A. Arpornwichanop, *Comput. Chem. Eng.* **2020**, *136*, 106805.
[13] J. Fu, T. Wang, X. Wang, J. Sun, M. Zheng, *Energy Procedia* **2017**, *105*, 4482–4491.
[14] T. Wang, J. Fu, M. Zheng, Z. Yu, *Appl. Energy* **2018**, *227*, 613–623.
[15] T. Sukkar, M. Skyllas-Kazacos, *J. Membr. Sci.* **2003**, *222*, 235–247.
[16] M. O. Bamgbopa, A. Fetyan, M. Vagin, A. A. Adelodun, *J. Energy Storage* **2022**, *50*, 104352.
[17] X. Li, J. Xiong, A. Tang, Y. Qin, J. Liu, C. Yan, *Appl. Energy* **2018**, *211*, 1050–1059.
[18] Y. Song, X. Li, C. Yan, A. Tang, *J. Power Sources* **2020**, *456*, 228004.
[19] Y. Song, X. Li, J. Xiong, L. Yang, G. Pan, C. Yan, A. Tang, *J. Power Sources* **2020**, *449*, 227503.
[20] J. Shin, B. Jeong, M. F. Chinannai, H. Ju, *Electrochim. Acta* **2021**, *390*, 138858.
[21] J. Shin, C. Kim, B. Jeong, N. Vaz, H. Ju, *J. Power Sources* **2022**, *526*, 231144.
[22] K. Wang, L. Liu, J. Xi, Z. Wu, X. Qiu, *J. Power Sources* **2017**, *338*, 17–25.
[23] A. Bhattarai, N. Wai, R. Schweiss, A. Whitehead, G. G. Scherer, P. C. Ghimire, T. M. Lim, H. H. Hng, *Appl. Energy* **2019**, *236*, 437–443.
[24] M.-Y. Lu, W.-W. Yang, X.-Y. Tang, Y.-H. Jiao, M. Ye, Q. Xu, *J. Energy Storage* **2021**, *44*, 103337.
[25] M.-Y. Lu, W.-W. Yang, X.-S. Bai, Y.-M. Deng, Y.-L. He, *Electrochim. Acta* **2019**, *319*, 210–226.
[26] W. Chen, J. Kang, *Chem. Phys.* **2020**, *529*, 110577.
[27] D. K. Kim, S. J. Yoon, J. Lee, S. Kim, *Appl. Energy* **2018**, *228*, 891–901.
[28] R. McCloy, Y. Li, J. Bao, M. Skyllas-Kazacos, *J. Process Control* **2022**, *115*, 36–47.
[29] B. Khaki, P. Das, *Electrochim. Acta* **2022**, *405*, 139842.
[30] S. Parsegov, M. Pugach, A. Polyakov, F. Ibáñez, *IFAC-PapersOnLine* **2022**, *55*, 187–192.
[31] J. Fu, T. Wang, X. Wang, J. Sun, M. Zheng, *Energy Procedia* **2017**, *105*, 4482–4491.
[32] A. Karrech, K. Regenauer-Lieb, F. Abbassi, *J. Energy Storage* **2022**, *45*, 103623.
[33] C. Sun, J. Chen, H. Zhang, X. Han, Q. Luo, *J. Power Sources* **2010**, *195*, 890–897.
[34] K. Oh, M. Moazzam, G. Gwak, H. Ju, *Electrochim. Acta* **2019**, *297*, 101–111.
[35] D. Reynard, C. R. Dennison, A. Battistel, H. H. Girault, *J. Power Sources* **2018**, *390*, 30–37.
[36] A. Fetyan, G. A. El-Nagar, I. Lauermann, M. Schnucklake, J. Schneider, C. Roth, *J. Energy Chem.* **2019**, *32*, 57–62.
[37] A. Fetyan, B. P. Benetho, M. O. Bamgbopa, *J. Energy Chem.* **2023**, *81*, 64–70.
[38] Y. Yang, Y. Zhang, L. Tang, T. Liu, S. Peng, X. Yang, *J. Power Sources* **2020**, *450*, 227675.
[39] S. Ressel, F. Bill, L. Holtz, N. Janshen, A. Chica, T. Flower, C. Weidlich, T. Struckmann, *J. Power Sources* **2018**, *378*, 776–783.
[40] K. W. Knehr, E. Agar, C. R. Dennison, A. R. Kalidindi, E. C. Kumbur, *J. Electrochem. Soc.* **2012**, *159*, A1446.

Manuscript received: July 10, 2023
Revised manuscript received: August 22, 2023
Accepted manuscript online: August 22, 2023
Version of record online: September 13, 2023

© 2023 Wiley-VCH GmbH

25666223, 2023, 11, Downloaded from https://chemistry-europe.onlinelibrary.wiley.com/doi/10.1002/batt.202300301 by University of Ulsan, Wiley Online Library on [11/11/2025]. See the Terms and Conditions (https://onlinelibrary.wiley.com/terms-and-conditions) on Wiley Online Library for rules of use; OA articles are governed by the applicable Creative Commons License